

CHAPTER 86

Harmonic Generation and Transmission Past a Submerged Rectangular Obstacle

Andrew M. Driscoll¹, Robert A. Dalrymple² and Stéphan T. Grilli³

Abstract : Experiments were conducted in a wave flume to study the harmonic evolution of a normally incident linear monochromatic wave train as it propagated over a submerged impermeable obstacle of rectangular cross-section. The reflection and transmission characteristics of the system were studied and compared to a linear scattering model, which was found to overpredict the transmission coefficients. The experiment was also simulated using the fully nonlinear model by Grilli *et al.* (1989), which performed well given its inviscid potential assumptions.

Introduction

The scenario of a linear wave train impinging on a submerged rectangular obstacle may be considered as a simplified representation of numerous physical phenomena, such as wave reflection and transformation over offshore reefs, bars and submerged breakwaters, which occur along actual coastlines. For this reason, the situation has been studied by numerous authors in the past 30 years, including Takano (1960), Mei and Black (1969), Losada (1991) and Rey *et al.* (1992), with the aim of analytically predicting the reflection and transmission characteristics for a given incident wave condition and obstacle geometry.

These authors have considered the problem completely in the linear context; an incident linear wave is partially reflected upon passing a submerged rectangular obstacle, with both transmitted and reflected energy propagating at the same frequency as the incident wave.

¹Arctec Offshore Corporation, Escondido, CA 92025

²F. ASCE, Director, Center for Applied Coastal Research, University of Delaware, Newark, DE 19716

³M. ASCE, Department of Ocean Engineering, University of Rhode Island, Kingston, RI 02881

Such assumptions become suspect as $\mu (= kh)$ becomes small and $\delta (= a/h)$ becomes large over the obstacle. Under these circumstances, significant harmonic generation may occur over the obstacle, as has been observed by Seelig (1980) and Rey *et al.* (1992). The wave condition found downwave of the obstacle for such a nonlinear situation is likely to have energy distributed not only at the fundamental frequency, but at a number of higher harmonic frequencies as well.

The goals of this research are : (i) to perform a series of laboratory experiments to scrutinize the spectral transformation which occurs when a linear wavetrain passes over a submerged rectangular obstacle; (ii) determine the performance of the standard linear scattering theory for a situation where nonlinearity is significant over the obstacle; and (iii) to evaluate the ability of the fully nonlinear potential model by Grilli *et al.* (1989) to simulate the laboratory data.

Experimental setup

The experiments were conducted in a precision wave flume with dimensions 30 m long by 0.6 m wide by 1 m deep. Repeatable wave trains were generated with a computer-controlled horizontal piston wavemaker, and a 1:35 impermeable slope at the opposite end of the tank functioned as a wave absorber. A submerged impermeable rectangular obstacle the width of the flume was fixed to the bottom of the tank 7.0 m from the wavemaker paddle. The water depth was $h_o = 0.5$ m, and the obstacle depth was $h_1 = 0.12$ m, so that the obstacle vertical aspect ratio is $\frac{h_o - h_1}{h_o} = 0.76$. The obstacle length was 0.78 m, i.e., $1.58h_o$ or slightly more than twice its height.

Two sets of experiments were carried out. In the first experimental set, a single sine wave condition (incident height $H_i = 2.50$ cm, period $T = 1.70$ s, with $ka = 0.019$) was produced on seven occasions. By moving the position of four wave gages prior to each run, an array of 28 gage locations was created (fig. 1).

The second experimental set consisted of 12 additional runs with the same wave height but with wave periods ranging from 0.8 s to 1.9 s. A 3-gage array was placed between the obstacle and the wave generator, thereby allowing the reflection coefficient (K_r) to be determined as a function of the incident wavenumber (fig. 2). Two additional gages were placed at locations downwave of the obstacle for redundant measurement of the transmission coefficient (K_t).

Experimental results

Spectral analyses of the 28 wave gage locations in the experimental data set yield the amplitudes of the individual harmonics, and reveal the nonlinear transformation undergone as incident linear waves pass over the obstacle (fig. 3). It is seen that significant harmonic generation occurs over the obstacle, and that

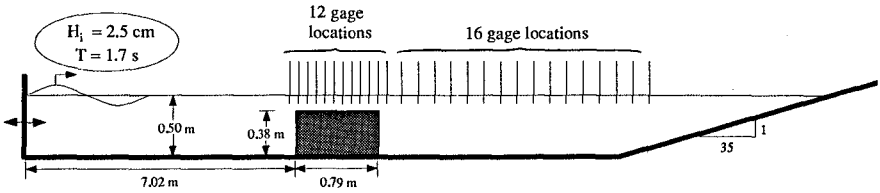


Figure 1: Experimental setup for spectral evolution portion of experiments.

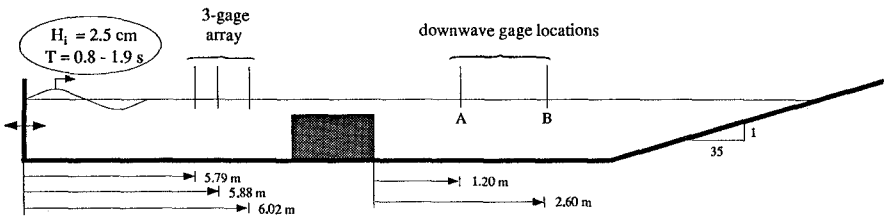


Figure 2: Experimental setup for reflection/transmission portion of experiments.

spatial amplitude modulation is present downwave of the obstacle. Such downwave amplitude modulations are certainly not due to reflection-induced partial standing waves, as reflection from the 1:35 slope is quite small (measured at less than 2 % at the first harmonic frequency). It must thus be concluded that the situation downwave of the obstacle is still quite dynamic with respect to harmonic evolution.

Comparison: linear scattering model vs. experiment

As the wave condition downwave of the obstacle has been shown to be both nonlinear and spatially varying, it is of interest to compare the experimentally measured values of K_r and K_t to those predicted analytically by a linear scattering model such as that of Losada (1991). The comparison, given in fig. 4, shows that the linear model predicts K_r quite well, but consistently overpredicts K_t . This overprediction is presumably due to the transfer of energy to the higher harmonics, and also to frictional and turbulent losses. From fig. 4, it is also seen that the measured value of K_t varied between gage location A and gage location B by as much as 5 % or more.

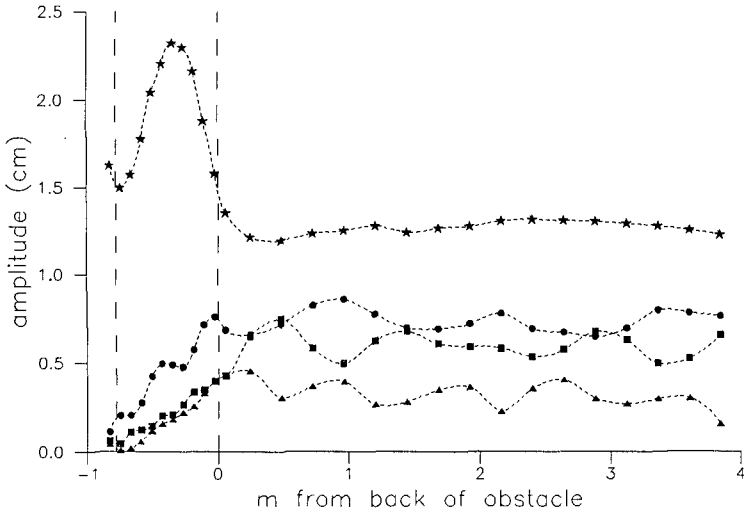


Figure 3: Spatial evolution of the first four harmonics in the experimental data; (\star)=1st harmonic, (\bullet)=2nd harmonic, (\blacksquare)=3rd harmonic, (\blacktriangle)=4th harmonic. Fine dashed lines are splines fit to data points, long dashed lines show boundaries of obstacle.

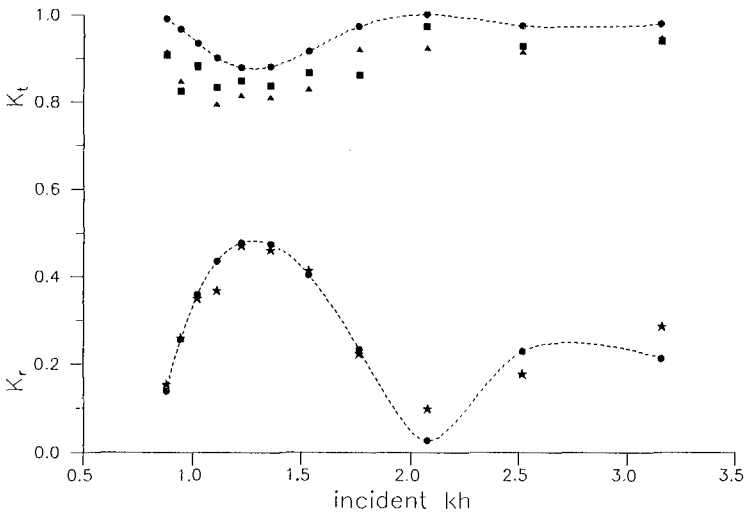


Figure 4: Comparison of K_r and K_t found experimentally and via the linear model of Losada (1991); (\bullet)=results of Losada (1991) model, (\star)=measured K_r , (\blacktriangle)=measured K_t at gage A, (\blacksquare)=measured K_t at gage B. Dashed lines are splines fit to Losada data.

Boundary element method (BEM) model

The two-dimensional nonlinear potential model by Grilli *et al.* (1989,1990), and its most recent extensions, are used to compute wave propagation over the submerged obstacle. With the velocity potential being defined as $\phi(x, t)$, the velocity is given by $u = \nabla\phi = (u, w)$, and the continuity equation in the fluid domain $\Omega(t)$ with boundary $\Gamma(t)$, is a Laplace's equation for the potential,

$$\nabla^2\phi = 0 \quad \text{in } \Omega(t) \quad (1)$$

Using the free space Green's function $G(x, x_l) = -\frac{1}{2\pi} \log |x - x_l|$, equation (1) is transformed into a Boundary Integral Equation (BIE),

$$\alpha(x_l)\phi(x_l) = \int_{\Gamma(x)} \left[\frac{\partial\phi}{\partial n}(x)G(x, x_l) - \phi(x)\frac{\partial G(x, x_l)}{\partial n} \right] d\Gamma(x) \quad (2)$$

where $x = (x, z)$ and $x_l = (x_l, z_l)$ are position vectors for points on the boundary, n is the unit outward normal vector, and $\alpha(x_l)$ is a geometric coefficient.

On the free surface $\Gamma_f(t)$, ϕ satisfies the full nonlinear kinematic and dynamic boundary conditions,

$$\frac{Dr}{Dt} = \left(\frac{\partial}{\partial t} + u \cdot \nabla \right) r = u = \nabla\phi \quad \text{on } \Gamma_f(t) \quad (3)$$

$$\frac{D\phi}{Dt} = -g\eta + \frac{1}{2}\nabla\phi \cdot \nabla\phi - \frac{p_a}{\rho} \quad \text{on } \Gamma_f(t) \quad (4)$$

respectively, with r , the position vector of a free surface fluid particle, g the acceleration due to gravity, η the vertical elevation of the free surface (positive upwards and $\eta = 0$ at the undisturbed free surface), p_a the pressure at the surface, and ρ the fluid density.

No-flow conditions are prescribed along solid boundaries, and, in the present applications, cnoidal waves are generated on the boundary $\Gamma_{r1}(t)$ by specifying a piston wavemaker motion, as in laboratory experiments (see Grilli & Svendsen 1990, for detail).

The time integration : The time stepping, follows the Eulerian-Lagrangian approach used by Dold & Peregrine 1984. It consists of integrating free surface conditions (3) and (4) at time t , to establish both the new position of the free surface $\Gamma_f(t)$, and the boundary conditions at time $t + \Delta t$ (Δt denotes a small time step increment). Second-order Taylor expansions are expressed in terms of Δt and of the Lagrangian time derivative (as defined in (3)), for both the position $r(t)$ and the potential $\phi(t)$ on the free surface. Coefficients in the series

are calculated by solving two Laplace problems—for ϕ and $\frac{\partial\phi}{\partial t}$ —at each time step (see detail in Grilli, *et al.* 1989).

Numerical implementation : The BIE (2), equivalent to Laplace problems (1) for ϕ , and the equivalent BIE problem for $\frac{\partial\phi}{\partial t}$ are solved by a higher-order BEM, using a set of collocation nodes on the boundary, and elements to interpolate between collocation nodes. Quasi-spline elements are used on the free surface, and isoparametric quadratic elements elsewhere. Each integral in (2) is transformed into a sum of integrals over each boundary element. Non-singular integrals are calculated by standard Gauss quadrature rules. A kernel transformation is applied to the weakly singular integrals, which are then integrated by a numerical quadrature exact for the logarithmic singularity. Details of the numerical implementation can be found in Grilli, *et al.* 1990, along with a discussion of corner problems associated with surface piercing bodies such as wavemakers.

Discretization and numerical parameters : A limitation of the BEM model is that any wave breaking in the computational domain effectively halts the solution algorithm. An adjustment of tank boundaries, hence, had to be made to prevent breaking on the slope of the numerical wave flume. Tank boundaries were re-defined such that the most downwave portion of the slope made the transition to a shallow shelf just below the breaking depth. Fig. 5 shows the re-defined tank boundaries which includes a region of constant depth $h_o = 1$ and length $21h_o$, and a 1:35 slope with a shelf of constant depth $h_1 = 0.34$, at the upper part of the slope, from $x' = \frac{x}{h_o} = 44$ to 56. A rectangular bar of height $0.76h_o$ and width $1.58h_o$ is located with its axis at $x' = 14.83$. As a transmitting boundary condition was not available in the model, reflection off the back wall of the numerical wave flume became a limiting condition. The comparison of BEM model vs. experiments must thus be made in the time between the initiation of paddle motion and the arrival of back wall-reflected energy at the most downwave gage location in the BEM model ($x' = 21$).

The free surface discretization is made of 224 quasi-spline elements, and there are 73 quadratic elements on the bottom and lateral boundaries. The interval between nodes on the free surface is 0.25, and 0.50 on the horizontal bottom, the slope, and the shelf bottom. To increase resolution and accuracy on and above the bar, this interval is reduced to about 0.20 along the bar three sides. The total number of nodes is 365. This corresponds to a CPU time of 7.63sec (IBM3090/300) per time step. Time step is automatically selected in the model, to ensure optimum accuracy and stability of calculations.

BEM model vs. experiment

A comparison is made between computations and experiments, for which both experimental and numerical set-ups correspond to closely identical conditions, with the waves being generated from still water using a piston wavemaker in

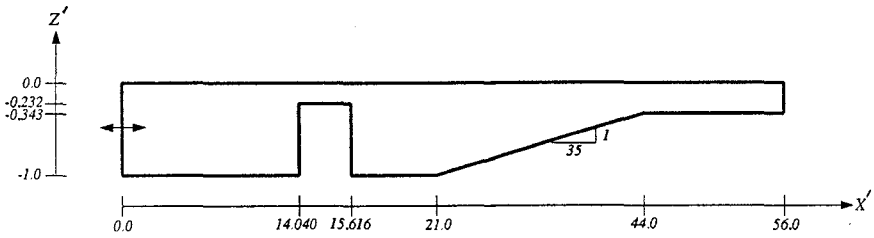


Figure 5: Geometry of the numerical wave flume, as re-defined for entry into BEM model. The shown axes are nondimensionalized with the water depth, $x' = x/h$ and $z' = z/h$.

both cases. In the present case, a cnoidal wave of height $H'_i = \frac{H_i}{h_o} = 0.05$, and period $T' = T\sqrt{\frac{g}{h_o}} = 7.52$ is generated at the leftward lateral boundary of the computational domain, and the corresponding incident wave profile is within 2% of a simple sine wave of length $\frac{L}{h_o} = 6.75$, as measured in the experiments. The model is run for over 20 wave periods, and no adjustment of time lag between both data sets is made before comparison. This, hence, represents a very demanding test of the model performance.

Fig. 6 shows a water surface comparison between the experimental and BEM results. A similar comparison is shown in fig. 7 for time series at locations 0.72 m and 1.92 m downwave of the obstacle. The BEM results are seen to deviate from the experimental results in both amplitude and phase. The nature of this deviation is better revealed by a frequency-domain comparison (fig. 8) which, due to the limitation of the non-breaking BEM requirement, is possible only for the first 8 waveforms following a 10-second startup period. The BEM model is shown to predict harmonics of similar amplitude to those observed in the experiments, with the exception of the first harmonic, which is overpredicted.

This discrepancy in first harmonic amplitude is likely due to the influence of flow separation as the wave-induced velocity oscillations interacted with the corners of the submerged obstacle. As such flow separation was observed in the experiments, the disagreement in the first harmonic amplitude between the BEM model and experiment is not surprising, given the inviscid potential flow assumptions of the model.

As a check, the flow separation loss incurred as a waveform passes the obstacle may be estimated with a crude analytical approach. A simple nonlinear friction representation is assumed, $\eta_1 - \eta_2 = \frac{f}{2g}|u|u$. If the obstacle is assumed thin in relation to the wavelength, quasi-steady flow is assumed, and frictional

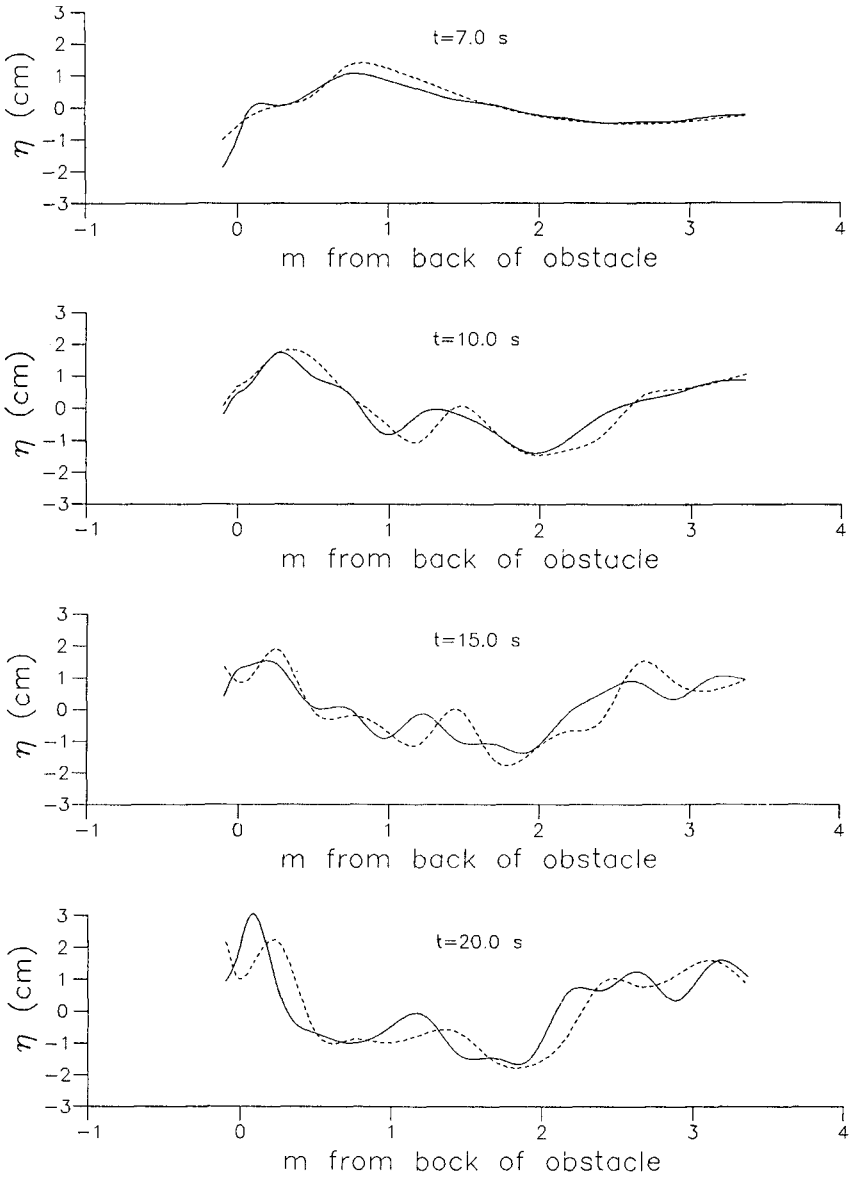


Figure 6: Water surface comparison of BEM model to experiment at $t=7.0$ s, $t=10.0$ s, $t=15.0$ and $t=20.0$ s after the initiation of paddle motion; (---)=BEM model, (—)=experiment.

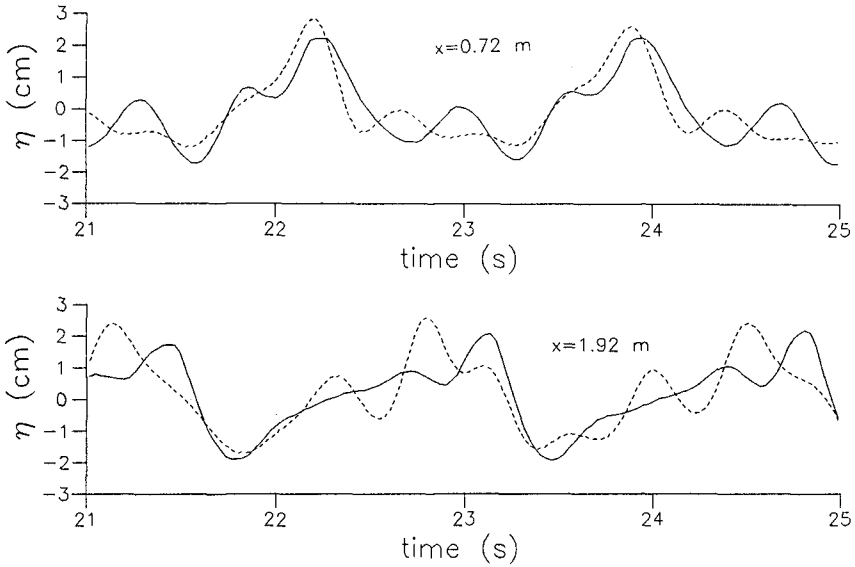


Figure 7: Time series comparison of BEM model data to experiment, at locations 0.72 m and 1.92 m downwave of obstacle; (---)=BEM model, (—)=experiment.

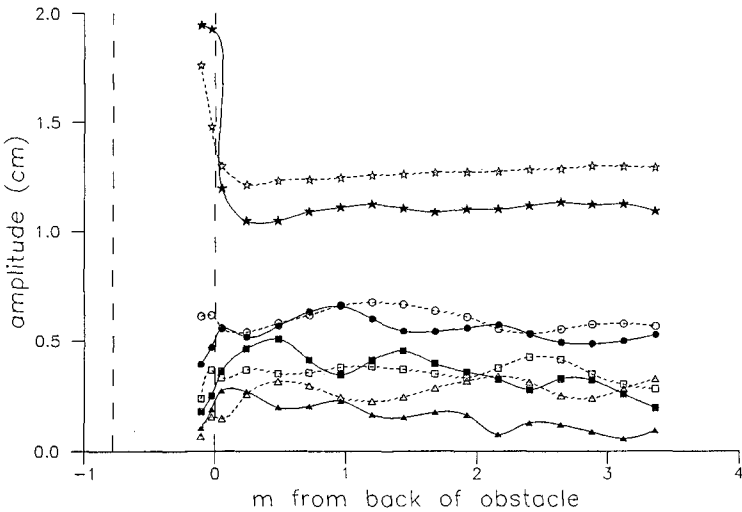


Figure 8: Comparison of spatial amplitude modulations, BEM model and experiment; (---)=BEM model, (—)=experiment, (★, ☆)=1st harmonic, (●, ○)=2nd harmonic, (■, □)=3rd harmonic, (▲, △)=4th harmonic.

effects are averaged over a wavelength, it may be shown that

$$\eta_1 - \eta_2 = \frac{4(h/h_o - 1)^2 a^2}{3\pi h_o^2 \omega^2 \cosh^2 kh} [\sinh kh - \sinh k(h - h_o)]^2 \quad (5)$$

where η_1 and η_2 are the water surface elevations prior to and after the obstacle, f is an empirical friction-loss coefficient, u is the amplitude of the depth-averaged velocity downwave of the obstacle, a and h are the amplitude and depth behind the obstacle and h_o is the depth on top of the obstacle. The friction coefficient f for this case is given by $f = (h/h_o - 1)^2$.

Introducing the downwave first harmonic amplitude from the BEM results (~ 1.25 cm) and the other relevant parameters into 5, we find $\eta_1 - \eta_2 \simeq 0.16$ cm. This agrees well with the discrepancy between BEM and experimental amplitudes of approx 0.15 cm.

The downwave higher harmonic amplitude modulations are less pronounced in fig. 8 compared to fig. 3, when the tank was fully developed. Nonetheless, the BEM model does predict spatial amplitude modulations which are qualitatively similar to the experimental results. The degree of disagreement present is certainly also due to the influence of flow separation at the first harmonic frequency, as a misrepresentation of the first harmonic component will be passed on as erroneously simulated higher harmonics as well.

Conclusions

The spectral evolution of an incident regular wave train has been traced as it propagated over a submerged rectangular obstacle, and comparisons have been made between the experimental data and both a traditional linear scattering model and a BEM model. The experimental data revealed the existence of spatial amplitude modulations downwave of the obstacle.

The linear model of Losada (1991) was shown to predict the reflection coefficient quite well, despite the high degree of nonlinearity present in the vicinity of the obstacle. However, it was seen that the transmission coefficient was consistently overpredicted due the linear model's omission of energy transfer to higher harmonics and energy dissipation. An implication of the above results is that the linear scattering approach may underestimate the effectiveness of a structure (ie, submerged breakwater) under highly nonlinear situations.

The BEM model by Grilli *et al.* (1989) was found to simulate downwave spatial amplitude modulations qualitatively similar to those found in the data. Comparisons, however, were hampered by the presence of flow separation in the experiments which could not be modelled in the BEM formulation. It is conjectured that the BEM model would have simulated the experiments more ac-

curately, had the obstacle depth been greater, thus inducing less flow separation.

References

- Dold, J.W. and D.H. Peregrine (1984). Steep unsteady water waves: an efficient computational scheme. *Proceedings of the 19th International Coastal Engineering Conference*, ASCE, Houston, 955-967.
- Grilli, S.T., J. Skourup and I.A. Svendsen (1989). An efficient boundary element method for nonlinear water waves, *Engineering Analysis with Boundary Elements*, **6**, 97-107.
- Grilli, S.T. and I.A. Svendsen (1990) Corner Problems and Global Accuracy in the Boundary Element Solution of Nonlinear Wave Flows, *Engineering Analysis with Boundary Elements*, **7**(4), 178-195.
- Longuet-Higgins, M.S. and E.D. Cokelet (1976). The deformation of steep surface waves on water - I: a numerical method of computation, *Proceedings of the Royal Society of London*, **A350**, 1-26.
- Losada, I. (1991) Estudio de la propagacion de un tren lineal de ondas por un medio discontinuo, Ph.D. dissertation, University of Cantabria, Santander, Spain.
- Mei, C.C. and J.L. Black (1969). Scattering of surface waves by rectangular obstacles in waters of finite depth, *Journal of Fluid Mechanics*, **28**, 499-511.
- Rey, V., M. Belzons and E. Guazzelli (1991). Propagation of surface gravity waves over a rectangular submerged bar, *Journal of Fluid Mechanics*
- Seelig, W.N. (1980). Two-dimensional tests of wave transmission and reflection characteristics of laboratory breakwaters, Technical Report no. 80-1, USAE Coastal Engineering Research Center, Fort Belvoir, VA.
- Takano, K. (1960). Effets d'un obstacle parallepipédique sur la propagation de la houle, *La Houille Blanche*, **2**, 247-267.